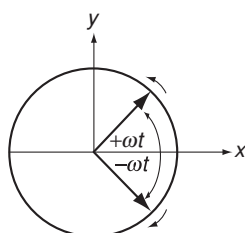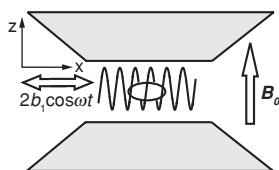# 9   Magnetic resonance

Resonance arises when the energy levels of a quantized system of electronic or nuclear moments are Zeeman split by a uniform magnetic field and the system absorbs energy from an oscillating magnetic field at sharply defined frequencies, which correspond to transitions between the levels. Classically, resonance occurs when a transverse AC field is applied at the Larmor frequency. Resonance methods are valuable for investigating the structure and magnetic properties of solids, and they are used for imaging and other applications. The resonant moment may be an isolated ionic spin or free radical, as in electron paramagnetic resonance (EPR), or a nuclear spin as in nuclear magnetic resonance (NMR). Otherwise it can be the ordered magnetization as in ferromagnetic resonance (FMR). Resonant effects are also associated with spin waves, and domain walls. The related techniques of Mössbauer spectroscopy and muon spin resonance provide further information on hyperfine interactions in solids.

An AC field is decomposed into two counter-rotating fields.

A typical magnetic resonance experiment.

A magnetic system placed in a uniform magnetic field $\boldsymbol{B}_0$ may absorb electromagnetic radiation at a precisely defined frequency $\nu_0 = \omega_0/2\pi$ which falls in the radio-frequency or microwave range. The phenomenon is related to the Larmor precession of the magnetic moment, introduced in §3.2.2. In order to observe the resonance, an experimental geometry with *crossed* magnetic fields is needed. The steady uniform field defines the z-direction, while a high-frequency AC field $b_x = 2b_1 \cos \omega t$ is applied in the perpendicular plane. It is helpful to think of b_x as the sum of two counter-rotating fields $2b_1 \cos \omega t = b_1(\mathrm{e}^{\mathrm{i}\omega t} + \mathrm{e}^{-\mathrm{i}\omega t})$. Resonance occurs when the precession is synchronized with the clockwise or anticlockwise component. No resonance occurs when $\boldsymbol{b}_1$ is parallel to $\boldsymbol{B}_0$.

There is a vast literature on magnetic resonance. It formed the basis of the fifth age of magnetism, which flowed from understanding the quantum mechanics of angular momentum, and the development of microwaves for radar in the Second World War. The resonant system is an ensemble of free radicals or ions with unpaired electron spins in electron paramagnetic resonance (EPR) – also known as electron spin resonance (ESR). The entire coupled magnetic moment may resonate in ferromagnetic resonance (FMR), or else it can be the sublattice moments which precess in antiferromagnetic resonance (AFMR). The nuclei carry tiny moments that resonate at relatively low frequencies in nuclear magnetic resonance (NMR). Other resonances are related to spin waves, domain walls and conduction electrons. In magnetically ordered material, it may

be possible to observe the resonance without recourse to an external field B_0, making use of the internal demagnetizing or hyperfine fields.

These are all remarkable physical phenomena in their own right, but from our viewpoint magnetic resonance is interesting for the insight it provides into the magnetism of solids, and for applications such as high-frequency switching of magnetization and magnetic resonance imaging (MRI).

The resonant magnetic systems are usually small quantum objects – ions or electrons or nuclei with unpaired spin – so it is natural to adopt a picture of resonant transitions between quantized, Zeeman split energy levels. Nevertheless, the classical picture of excitation at the natural Larmor precession frequency, which is needed for macroscopic magnets, provides invaluable insights for the quantum systems too.

Think of the simplest case of an ion with magnetic moment m which is associated with an electronic angular momentum $\hbar S$. The constant of proportionality is the gyromagnetic ratio γ:
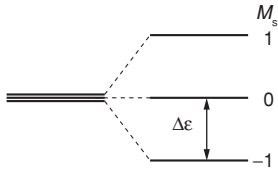
$$\mathfrak{m} = \gamma \hbar S, \tag{9.1}$$

where γ has units of $s^{-1}\,T^{-1}$ (hertz per tesla) and S is dimensionless. Both m and S are vector operators. The equation, which reads like a classical vector equation, really means that all of the corresponding matrix elements of m and S are proportional. The Zeeman interaction $\mathfrak{m} \cdot B_0$ in the steady field B_0 applied along Oz is represented by the Hamiltonian

$$\mathcal{H}_Z = -\mathfrak{m} \cdot B_0 = -\gamma \hbar B_0 S_z. \tag{9.2}$$

Eigenvalues are a set of equally spaced energy levels at

$$\varepsilon_i = -\gamma \hbar B_0 M_s; \qquad M_s = S, S-1, \ldots, -S. \tag{9.3}$$

The level spacing is $\Delta\varepsilon = \gamma \hbar B_0$. Magnetic dipole transitions between adjacent levels can be expected for radiation of angular frequency ω_0, where $\Delta\varepsilon = \hbar\omega_0$. Hence the resonance condition

$$\omega_0 = \gamma B_0 \tag{9.4}$$

does not depend on Planck's constant, which suggests it should be possible to deduce the same result by a classical argument. Note that γ for electrons is negative on account of their negative charge so the $M_s = -S$ level is lowest.

The torque on the magnetic moment m in a field B_0 is $\Gamma = \mathfrak{m} \times B_0$. This is equated to the rate of change of angular momentum $d(\hbar S)/dt$. Hence the equation of motion is[1]

$$\frac{d\mathfrak{m}}{dt} = \gamma \mathfrak{m} \times B_0. \tag{9.5}$$

Zeeman split enegy levels for an electronic system with $S = 1$.

[1] This and similar equations appear with a negative sign, if the convention is adopted that e, rather than $-e$, is the charge on the electron.

B

dm

m

θ

$\Gamma = m \times B$

Precession of a magnetic moment in an applied field.
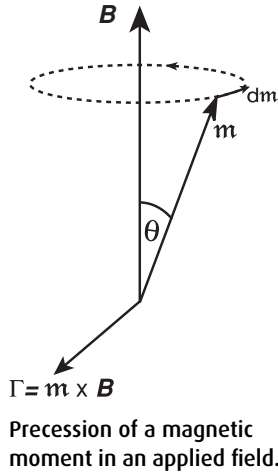
Now dm, the change of m in a short time interval dt, is a vector perpendicular to both m and B_0, hence the moment precesses around the field, at angular frequency

$$\omega_0 = \gamma B_0.$$

This is the classical Larmor precession and resonance occurs when the field b_1 turns at the Larmor frequency.

The requirement that b_1 be applied perpendicular to B_0 for resonant absorption also follows from quantum mechanics. The Zeeman Hamiltonian (9.2) in matrix notation is diagonal with eigenstates $|M_S\rangle$. Adding an extra field in the z-direction merely changes the eigenvalues, but does not induce any transition between the states, because the off-diagonal matrix elements which mix different states are all zero. However, if b_1 is applied in the x-direction, the Hamiltonian becomes

$$\mathcal{H} = -\gamma \hbar (B_0 S_z + b_1 S_x). \tag{9.6}$$

The matrix representing S_x (§3.1.4) has non-zero off-diagonal elements $[n, n \pm 1]$. It can be expressed in terms of the ladder operators S^+ and S^- so it mixes states with $\Delta M_s = \pm 1$. At resonance, the AC magnetic field provokes transitions between the states which differ by $\Delta M_s = \pm 1$. This is known as the dipole selection rule.

9.1 Electron paramagnetic resonance

The Larmor precession frequency for electron spin is $f_L = \omega_L/2\pi = (ge/4\pi m_e)B$. Since $g = 2.0023$, the value of γ for free electrons, $-(ge/2m_e)$, is 176.1×10^9 s^{-1} T^{-1} and f_L is 28.02 GHz T^{-1}. Resonance occurs in the microwave range for fields produced by laboratory electromagnets. X-band (~ 9 GHz) microwaves with wavelength $\Lambda = c/\nu = 33$ mm are commonly employed, so the resonance is at about 300 mT. Sometimes Q-band (~ 40 GHz) radiation is used and the resonance field is correspondingly bigger. The sample is placed in a resonant cavity at the end of a waveguide, in a steady field. The cavity, operates in a TM$_{100}$ mode and delivers the requisite transverse magnetic field b_1.

Zeeman splitting of the energy levels for an isolated electron is $\gamma \hbar B_0 = g\mu_B B_0$, an energy that is small compared with $k_B T$ when $B_0 = 300$ mT. ($\mu_B/k_B = 0.673$ K T^{-1}) so the equilibrium population difference between the $M_S = \pm\frac{1}{2}$ sublevels is tiny. The spin polarization $(N_\uparrow - N_\downarrow)/(N_\uparrow + N_\downarrow)$ is
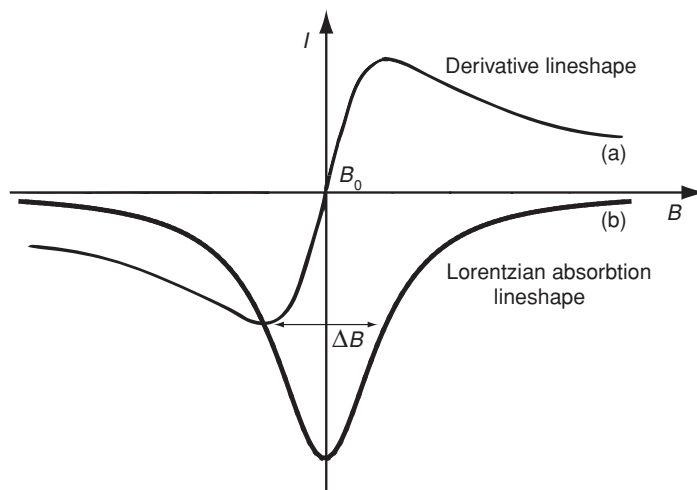
$$P = (1 - e^{-g\mu_B B/k_B T})/(1 + e^{-g\mu_B B/k_B T}).$$

(a) An EPR trace showing the derivative of the microwave absorption obtained when sweeping the DC field at a constant rate. **(b)** The absorption line obtained by integration.
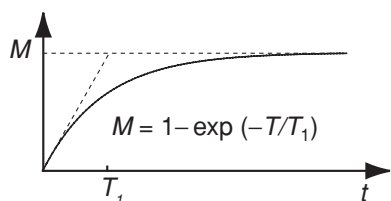
Spin-lattice relaxation of the magnetization towards its equilibrium value after saturating the resonance.

Conventionally the ↑ states are always those with their *moments* parallel to the applied field; they are those with $M_S = -\frac{1}{2}$ in this case.[2] The value of $P \approx g\mu_B B_0 / 2k_B T$ in 300 mT at room temperature is only 7×10^{-4}, so a sensitive detection method is needed to observe the resonance. It is often more convenient to sweep the magnetic field rather than the microwave frequency. Sensitivity is increased by using field modulation coils and detecting the absorbed power at the modulation frequency with a lock-in amplifier. The measured trace is the derivative of the absorption as a function of field (Fig. 9.1). The absorption line is the integral of this signal.
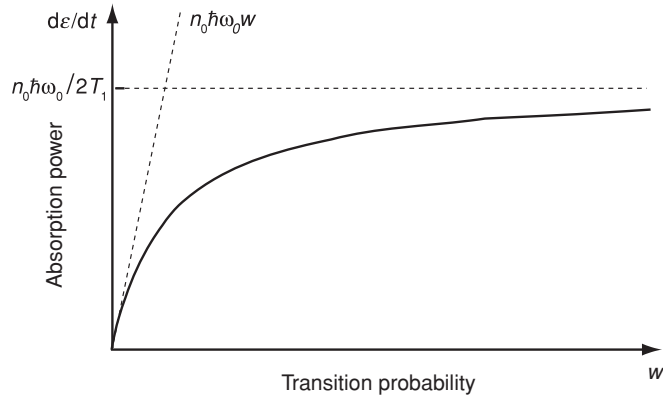
Measured parameters in EPR are the intensity of the resonance, its position B_0 which is normally expressed as an effective g-factor $g_{eff} = \hbar\omega_0 / \mu_B B_0$, where ω_0 is the resonance frequency, and the linewidth ΔB (full width at half maximum). The cavity resonance is very sharp, so the linewidth is determined by the sample.

Absorption of radiation is a dynamic process, which tends to equalize the Boltzmann populations of the levels. This tendency is counter-balanced by the desire of the spin system to regain its thermal equilibrium. The temperature T of the system is defined by the crystal lattice, so the exchange of energy between the spins and the lattice which is involved in thermalization is known as spin-lattice relaxation. The linewidth ΔB is inversely proportional to the spin-lattice relaxation time T_1. If T_1 is very short, the line becomes too broad to observe, whereas if T_1 is very long, the line is sharp, but its intensity becomes vanishingly small because the populations of the ↑ and ↓ states remain equal; there is no dissipation of energy. The order of magnitude of T_1 is provided by the

---

[2] The ↑ and ↓ states are referred to as 'spin up' and 'spin down' or more correctly as 'majority spin' and 'minority spin'. The meaning is that the moments of the ↑ electrons are aligned with the applied field, but their spin angular momentum is in the opposite direction, because of the negative charge of the electron.

uncertainty relation $\Delta\varepsilon\,\Delta t \approx \hbar$, so if $\Delta B = 1$ mT, $\Delta\varepsilon = g\mu_B\Delta B \approx 2\times10^{-26}$ J, $T_1 \approx 5\times10^{-9}$ s.

The probability w of transitions between the $\pm\frac{1}{2}$ levels stimulated by the microwave field is a quantity which is proportional to microwave power and identical for transitions in either sense. The rates of change of populations are

$$\frac{dN_\uparrow}{dt} = w(N_\downarrow - N_\uparrow) \quad \text{and} \quad \frac{dN_\downarrow}{dt} = w(N_\uparrow - N_\downarrow). \tag{9.7}$$

Subtracting these equations, and setting $N = N_\uparrow - N_\downarrow$, we find $dN/dt = -2wN$, which gives $N(t) = N(0)e^{-2wt}$. The populations tend to equalize at long times. The energy ε of the system is $N_\downarrow\hbar\omega_0$, so $d\varepsilon/dt = -\hbar\omega_0 w N(t)$. The rate of change of energy tends to zero at long times.

However, when we switch off the microwave power, the populations can be expected to relax to thermal equilibrium with longitudinal time constant T_1, so that $N(t) = N_0(1 - e^{-t/T_1})$, where N_0 is the equilibrium population difference. Taking relaxation into account, the rate of change of population imbalance becomes

$$\frac{dN(t)}{dt} = -2wN(t) + \frac{N_0 - N(t)}{T_1}. \tag{9.8}$$

There is a similar equation for the magnetization, since $M = N\mu_B/V$. In equilibrium, $dN(t)/dt = 0$, so $N(t) = N_0/(1 + 2wT_1)$. The rate of absorption of electromagnetic energy $N(t)\hbar\omega w$ is then

$$\frac{d\varepsilon}{dt} = \frac{N_0\hbar\omega_0 w}{1 + 2wT_1}, \tag{9.9}$$

which is plotted in Fig. 9.2. At low power, the rate of absorption is proportional to w, but at high power it saturates at a value proportional to $1/T_1$.

Spin-orbit interaction is the mechanism by which the spin system couples to the lattice phonon bath. Good EPR spectra are obtained with ions where the orbital moment is quenched or absent. The latter are S-state ions with half-filled shells, such as free radicals ($^2S_{1/2}$), Mn^{2+} or Fe^{3+} ($^6S_{5/2}$) and Eu^{2+} or
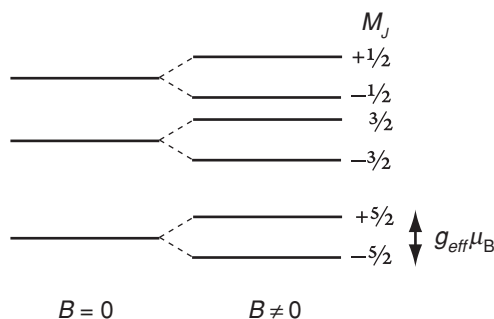
Gd^{3+} ($^8S_{7/2}$). Moreover, the resonant ions should be dilute in the crystal lattice to minimize dipolar and exchange interactions between them, which broaden the resonance linewidth and lead to dephasing of the spins.

The outer electrons of an ion interact strongly with the surrounding ions – the crystal-field interaction was discussed in §4.4. A crystal field of second order may include a term A_2^2 which mixes states where M_S (or, more generally, M_J) differs by 2. The fourth- or sixth-order crystal field may mix states where M_S differs by up to 4 or 6. These interactions are effective when $J > \frac{1}{2}$, $J > \frac{3}{2}$ and $J > \frac{5}{2}$, respectively. Although it is the ground state that is involved in EPR, the effect of the crystal field is to create a zero-field splitting of the energy levels which modifies the effective g-factor of the lowest energy level, and makes it anisotropic with respect to the crystal axes. The example of Ce^{3+}, a $4f^1$ Kramers ion with $J = \frac{5}{2}$, is shown in Fig. 9.3.

It is common practice in EPR to replace the Hamiltonian of the system by an effective spin Hamiltonian which describes how the ground-state energy level splits in a magnetic field. An effective spin S is chosen, so that the magnetic degeneracy is $2S + 1$. Terms in the spin Hamiltonian reflect the crystal symmetry of the resonant ion. Examples of terms to add to the Zeeman term in order to build the spin Hamiltonian are:

DS_z^2 for uniaxial symmetry;
$E(S_x^2 - S_y^2)$ for an orthorhombic distortion;
$D_c(S_x^4 + S_y^4 + S_z^4)$ for cubic symmetry.

Consider, for instance, the case of an ion with $S = 1$ in a site having uniaxial symmetry, with the field B_0 applied along the crystal axis. The spin Hamiltonian is

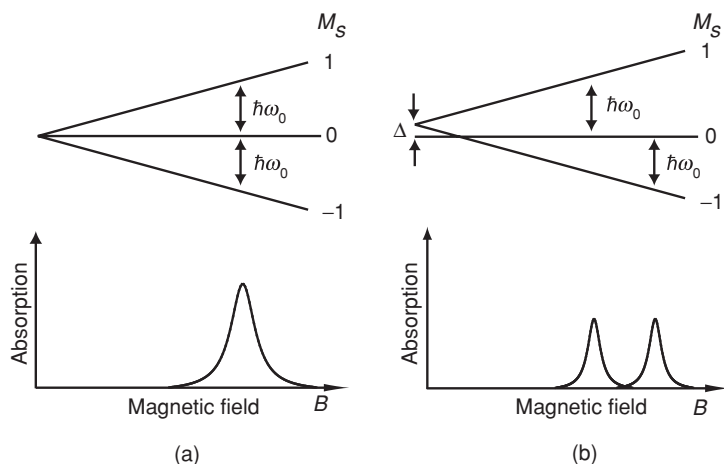$$\mathcal{H}_{spin} = DS_z^2 - g_{eff}\mu_B B_0 S_z. \tag{9.10}$$

The effect of the crystal field is to create fine structure in the EPR spectrum as shown in Fig. 9.4.

There is another interaction, of order 0.1 K at most, which modifies the splitting of the electronic ground state. This is the hyperfine interaction with the nucleus. The nucleus may possess quantized angular momentum $\hbar I$ when

the nuclear spin quantum number $I \neq 0$. The corresponding magnetic moment $\mathfrak{m}_n = g_n \mu_N I$ is about a thousand times smaller than the electronic moment; g_n is the nuclear g-factor, a number of order 1, and μ_N is the nuclear magneton:

$$\mu_N = e\hbar/2m_p = 5.0508 \times 10^{-27} \text{ A m}^2, \qquad (9.11)$$

where m_p is the proton mass. A magnetic field separates the $2I + 1$ degenerate nuclear energy levels with $M_I = I, I - 1, \ldots, -I$.

The unpaired electrons of a magnetic ion create a magnetic field at the nucleus, known as the hyperfine field. This ranges up to about 50 T in $3d$ ions, and it can be ten times larger for some rare-earths because of the $4f$ orbital contribution. These are huge magnetic fields, albeit in a very small volume. Hyperfine interactions are therefore of order 10^{-1}–10^{-3} K. They dominate the specific heat below 1 K and they give rise to hyperfine structure in EPR, NMR and Mössbauer spectra. The interactions are represented by the term $A\mathbf{I} \cdot \mathbf{S}$ in the spin Hamiltonian, with the hyperfine constant A having units of energy. Each degenerate M_S level splits into $(2I + 1)$ sublevels with energy $g\mu_B B_0 M_S + AM_I M_S$. Microwave transitions only occur between levels obeying the dipole selection rule $\Delta M_S = \pm 1$ or $\Delta M_I = 0$, since the frequencies required to induce transitions between the nuclear levels lie in the radio-frequency range – MHz rather than GHz. The resonances therefore occur at

$$\hbar\omega = [g\mu_B B_0(M_S + 1) + AM_I(M_S + 1)] - [g\mu_B B_0 M_S + AM_I M_S]$$
$$= g\mu_B B_0 + AM_I. \qquad (9.12)$$

Each EPR line therefore splits into $2I + 1$ hyperfine lines, as shown in Fig. 9.5.

EPR is normally applied to magnetic ions in insulators. However, it is possible to obtain a signal known as conduction electron spin resonance (CESR) from the free electrons in metals and semiconductors, provided the relaxation time is not too short.

(a) EPR transitions in the presence of hyperfine interactions, for an ion with $S = \frac{5}{2}$ and nuclear spin $I = \frac{5}{2}$. (b) EPR spectrum of Mn^{2+} impurities in Ga_2O_3, showing the hyperfine structure. (V. J. Folen, *Phys. Rev. B* **139**, A1961 (1965).)

(a)

5/2 ⟷ 3/2   −3/2 ⟷ −5/2

3/2 ⟷ 1/2   −1/2 ⟷ −3/2

1/2 ⟷ −1/2

(b)
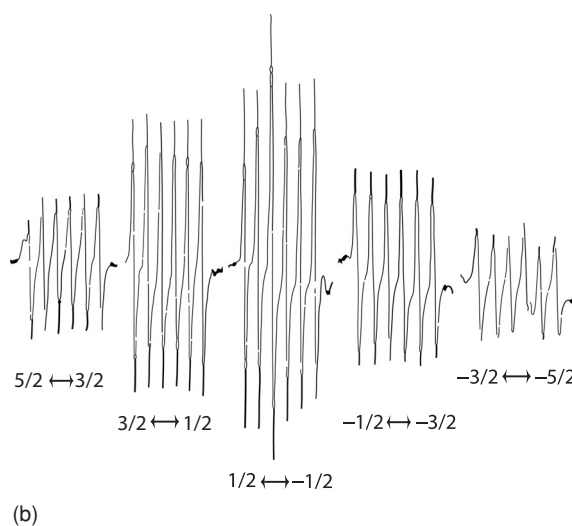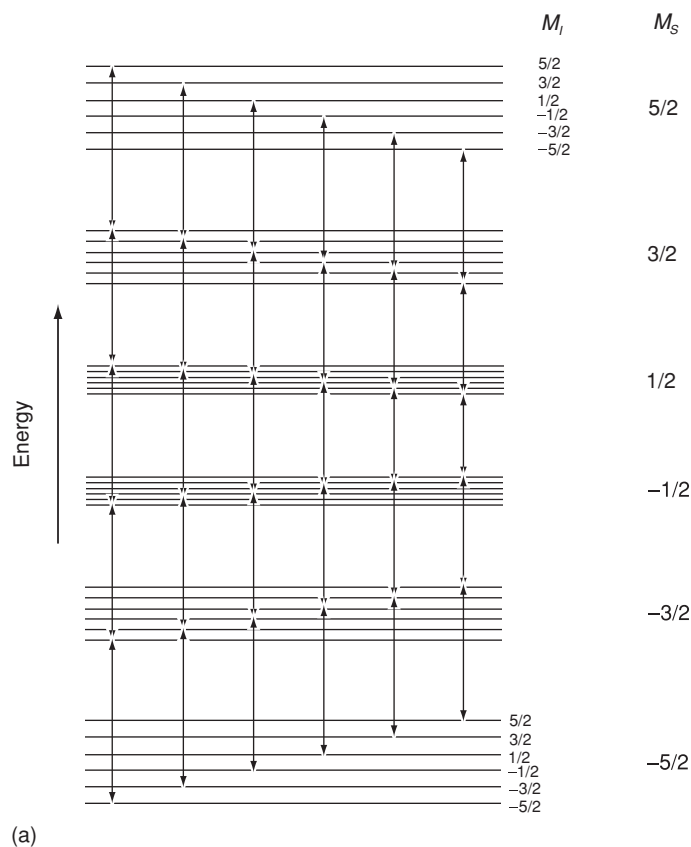
9.2 Ferromagnetic resonance

Resonance is also observed in the microwave frequency range when a *ferro-magnet* is subject to a uniform field $\boldsymbol{B}_0$ and a transverse high-frequency field $\boldsymbol{b}_1$. The system will be treated classically, like a giant spin, or macrospin. The magnetization of the sample is first assumed to remain uniform.

In the absence of damping the equation of motion is

$$\mathrm{d}\boldsymbol{M}/\mathrm{d}t = \gamma(\boldsymbol{M} \times \boldsymbol{B}'_0). \tag{9.13}$$

The magnetization precesses around the z axis at the Larmor frequency $f_L = \omega_0/2\pi$, where $\omega_0 = \gamma B_0$. Since the magnetization of the ferromagnet is largely due to the spin moments of the electrons, $\gamma \approx -(e/m_e)$, resonant frequencies for FMR are similar to those for EPR. The same apparatus is used for both.

If the precession is to be detected by resonant absorption of microwaves, high-frequency radiation has to be able to penetrate the specimen. This poses no difficulty for insulators such as ferrimagnetic oxides, but the skin depth of metallic iron at 10 GHz, for example, is only of order a micron so thin films or fine powder samples have to be used for metallic materials (12.2).

Furthermore, in ferromagnets we have to distinguish clearly the external field $\boldsymbol{H}' = \boldsymbol{B}'/\mu_0$ and the internal field $\boldsymbol{H} = \boldsymbol{H}' + \boldsymbol{H}_d$ present inside the ferromagnet. The demagnetizing field $\boldsymbol{H}_d = -\mathcal{N}\boldsymbol{M}$, where the demagnetizing tensor is assumed to be diagonal:

$$\mathcal{N} = \begin{bmatrix} \mathcal{N}_x & 0 & 0 \\ 0 & \mathcal{N}_y & 0 \\ 0 & 0 & \mathcal{N}_z \end{bmatrix}.$$

Provided $\boldsymbol{b}_1 \ll \boldsymbol{B}_0$, the magnetization is $\boldsymbol{M} \approx M_s\mathbf{e}_z + \boldsymbol{m}(t)$, where $\boldsymbol{m}(t) = \boldsymbol{m}_0\mathrm{e}^{\mathrm{i}\omega t}$ is the small in-plane component. The demagnetizing field is therefore

$$\boldsymbol{H}_d = -\mu_0[\mathcal{N}_x m_x\mathbf{e}_x + \mathcal{N}_y m_y\mathbf{e}_y + \mathcal{N}_z(m_z + M_s)\mathbf{e}_z]. \tag{9.14}$$

The oscillating components of magnetization $m = m_0\mathrm{e}^{\mathrm{i}\omega t}$ in the xy-plane are

$$\frac{\mathrm{d}m_x}{\mathrm{d}t} = \mu_0\gamma(m_y H_z - M H_y) = \mu_0\gamma[H'_0 + (\mathcal{N}_y - \mathcal{N}_z)M]m_y, \tag{9.15}$$

$$\frac{\mathrm{d}m_y}{\mathrm{d}t} = \mu_0\gamma(-m_x H_z + M H_x) = -\mu_0\gamma[H'_0 + (\mathcal{N}_x - \mathcal{N}_z)M]m_x, \tag{9.16}$$

where $M_z = M$. The external field $B'_0 = \mu_0 H'_0$ is applied in the z-direction. Solutions of these equations exist when

$$\begin{vmatrix} \mathrm{i}\omega & \gamma\mu_0[H'_0 + (\mathcal{N}_y - \mathcal{N}_z)M] \\ -\mu_0\gamma[H'_0 + (\mathcal{N}_x - \mathcal{N}_z)M] & \mathrm{i}\omega \end{vmatrix} = 0,$$

which leads to the Kittel equation for the resonance frequency:

$$\omega_0^2 = \mu_0^2\gamma^2[H'_0 + (\mathcal{N}_x - \mathcal{N}_z)M][H'_0 + (\mathcal{N}_y - \mathcal{N}_z)M]. \tag{9.17}$$

Table 9.1. g-factors for metallic ferromagnets	
Fe	2.08
Co	2.17
Ni	2.18
Gd	1.95

Special cases are:

- a sphere, $\mathcal{N}_x = \mathcal{N}_y = \mathcal{N}_z = \frac{1}{3}$, $\omega_0 = \gamma \mu_0 H_0'$;
- a thin film with H_0' perpendicular to the plane $\mathcal{N}_x = \mathcal{N}_y = 0$, $\mathcal{N}_z = 1$; $\omega_0 = \gamma \mu_0 (H_0' - M)$;
- a thin film with H_0' in plane $\mathcal{N}_y = \mathcal{N}_z = 0$, $\mathcal{N}_x = 1$; $\omega_0 = \gamma \mu_0 [H_0'(H_0' + M)]^{\frac{1}{2}}$.

Magnetocrystalline anisotropy also influences the ferromagnetic resonance frequency, so to the demagnetizing field in the above expressions may be added the anisotropy field, $H_a = 2K_1/M_s$. A sphere, for example, with the z axis as the easy anisotropy axis and $\mathcal{N}_x = \mathcal{N}_y = \mathcal{N}_z = \frac{1}{3}$ has resonance frequency $\omega_0 = \gamma \mu_0 (H_0 + 2K_1/M_s)$. It is possible to observe ferromagnetic resonance in *zero* external field for a single-domain particle, or a crystal of high-anisotropy material magnetized along Oz.

For a spherical sample with cubic anisotropy (§5.5.2), when H_0' is applied along [100], (9.17) applies with $K_1 = K_{1c}$. When H_0' is applied along [111]

$$\omega_0 = \gamma \mu_0 (H_0' - 4K_{1c}/3M_s - 4K_{2c}/9M_s), \qquad (9.18)$$

whereas if H_0 is applied along [110]

$$\omega_0 = \gamma \mu_0 [(H_0' - 2K_{1c}/M_s)(H_0' + K_{1c}/M_s + K_{2c}/2M_s)]^{\frac{1}{2}}. \qquad (9.19)$$

In the case of a thin film with an easy axis perpendicular to the plane of the film, the expression for the resonance frequency is

$$\omega_0 = \gamma \mu_0 (H_0' + 2K_1/M_s - M_s). \qquad (9.20)$$

Ferromagnetic resonance can therefore provide a measurement of M_s and K_i as well as γ. An advantage of the method is that the magnetization, or magnetic moment per cubic metre, is determined with no need to know the sample volume. The gyromagnetic ratio is related to the g-factor; $\gamma = -g\mu_B/\hbar$. Values of g for the metallic ferromagnets are given in Table 9.1. The ratio of orbital moment to spin moment is $\frac{1}{2}(g - 2)$.

The instantaneous field in the sample is uniform in an FMR experiment provided the wavelength of the microwaves is much greater than the sample size. At 10 GHz, $\lambda = 3$ cm, so the condition is satisfied for millimetre-size samples. However, the giant-spin assumption of uniform magnetization throughout the sample is not generally valid. Nonlinear magnetostatic modes may be excited.

Spin-wave resonance spectrum of permalloy (R. Weber and P. Tannenwald, *IEEE Trans. Maps.* **4**, 28 (1968)).
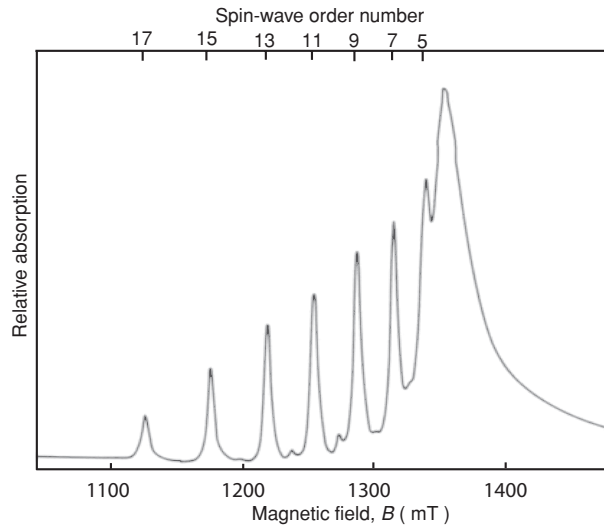
An example is the standing spin waves excited in thin ferromagnetic films when the steady field B_0 is applied normal to the film surface, Fig. 9.6. The in-plane radio-frequency field can excite modes with an odd number of half-wavelengths. Those with an even number do not couple with the field. Ferromagnetic spin waves follow the dispersion relation (5.56) $\hbar\omega_q = D_{sw}q^2$, where $q = n\pi/\text{t}$; n is an integer and t is the film thickness. Equation (9.17) becomes

$$\omega_q = \gamma\mu_0(H'_0 - M) + D_{sw}(n\pi/\text{t})^2/\hbar.$$

The spin-wave stiffness can be determined in this way.

9.2.1 Antiferromagnetic resonance

An antiferromagnet is composed of two equal and opposite sublattices, each of which is subject to an anisotropy field and an exchange field. The exchange field on the 'A' sublattice, for example, is $H_{exA} = -n_{AB}M_B$ (6.1), where n_{AB} is the molecular field coefficient. Solving the equations of motion for m_x, m_y for the two sublattices leads to the solution

$$\omega_0 = \gamma\mu_0[H_a(H_a + 2H_{ex})]^{\frac{1}{2}}. \tag{9.21}$$

Molecular field coefficients may take values of up to 100 T in antiferromagnets, so the resonance frequencies are very high, often in the 10^2–10^3 GHz range.

9.2.2 Damping

Precession mode for antiferromagnetic resonance.

Free precession of the magnetization in the internal field at frequency $\omega_0 = \gamma\mu_0 H$ cannot go on for ever. Eventually, the magnetization must align with the field. In EPR and NMR, this process involves spin-lattice relaxation of
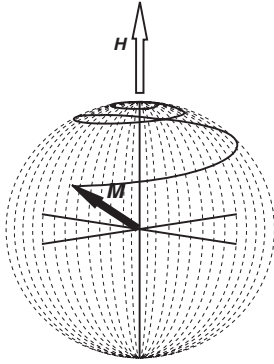
Precession of the magnetization in a field showing the effect of damping.

the quantum spin system. A way to represent the process for the macroscopic magnetization is to add a phenomenological damping term to the equation of motion. Two suggested forms, due to Landau and Lifschitz and Gilbert respectively, are:

$$\frac{\mathrm{d}\boldsymbol{M}}{\mathrm{d}t} = \gamma \boldsymbol{M} \times \boldsymbol{B}_0 - \gamma \frac{\lambda}{M} \boldsymbol{M} \times \boldsymbol{M} \times \boldsymbol{B}_0; \tag{9.22}$$

$$\frac{\mathrm{d}\boldsymbol{M}}{\mathrm{d}t} = \gamma \boldsymbol{M} \times \boldsymbol{B}_0 - \frac{\alpha}{M} \boldsymbol{M} \times \frac{\mathrm{d}\boldsymbol{M}}{\mathrm{d}t}. \tag{9.23}$$

When $\alpha \ll 1$, the two forms are equivalent, with $\lambda = \alpha$. A typical value of the Gilbert damping is $\alpha = 0.01$. The effect of damping is to make the precessing magnetization spiral in towards the direction of the applied field $\boldsymbol{B}_0$.

In the absence of damping, the equation of motion in component form is

$$\left(\frac{\mathrm{d}M_x}{\mathrm{d}t}, \frac{\mathrm{d}M_y}{\mathrm{d}t} \right) = \gamma \mu_0 H(M_y, -M_x). \tag{9.24}$$

Differentiating with respect to time,

$$\left(\frac{\mathrm{d}^2 M_x}{\mathrm{d}t^2}, \frac{\mathrm{d}^2 M_y}{\mathrm{d}t^2} \right) = \gamma \mu_0 H \left(\frac{\mathrm{d}M_y}{\mathrm{d}t}, -\frac{\mathrm{d}M_x}{\mathrm{d}t} \right) = \gamma^2 \mu_0^2 H^2 (-M_x, M_y). \tag{9.25}$$

Hence

$$\frac{\mathrm{d}^2 M_x}{\mathrm{d}t^2} = -\omega_0^2 M_x; \quad \frac{\mathrm{d}^2 M_y}{\mathrm{d}t^2} = \omega_0^2 M_y; \quad \frac{\mathrm{d}^2 M_z}{\mathrm{d}t^2} = 0. \tag{9.26}$$

The solution is a uniform precession

$$M_x = M_s \sin\theta \exp \mathrm{i}\omega_0 t; \quad M_y = M_s \sin\theta \exp(\mathrm{i}\omega_0 t + \pi/2); \quad M_z = M_s \cos\theta. \tag{9.27}$$

where the real parts represent the physical components of the magnetization. When Gilbert damping is taken into account, the equations of motion reduce to

Gilbert damping of a resonant oscillation.

$$\frac{\mathrm{d}M_x}{\mathrm{d}t} = \omega_0' \left[M_y + \alpha \frac{M_y M_z}{M_s} \right], \tag{9.28}$$

$$\frac{\mathrm{d}M_y}{\mathrm{d}t} = \omega_0' \left[-M_x + \alpha \frac{M_x M_z}{M_s} \right], \tag{9.29}$$

$$\frac{\mathrm{d}M_z}{\mathrm{d}t} = \omega_0' \left[-M_s + \alpha \frac{M_z^2}{M_s} \right], \tag{9.30}$$

where $\omega_0' = \omega_0/(1 + \alpha^2)$. These are spiralling solutions with $\omega \neq \omega_0$ and $\theta = \theta(t)$. Differentiating the expression (9.27) for M_x,

$$\frac{\mathrm{d}M_x}{\mathrm{d}t} = \mathrm{i}\omega M_s \sin\theta \exp \mathrm{i}\omega t + M_s \frac{\mathrm{d}\theta}{\mathrm{d}t} \cos\theta \exp \mathrm{i}\omega t \tag{9.31}$$

$$\frac{\mathrm{d}M_x}{\mathrm{d}t} = \omega M_y + \frac{M_y M_z}{\sin\theta M_s} \frac{\mathrm{d}\theta}{\mathrm{d}t}. \tag{9.32}$$

Hence $\omega = \omega_0'$ and $\mathrm{d}\theta/\mathrm{d}t = \omega_0' \alpha \sin\theta$.

Switching of the
magnetization of a
thin-film element. The
switching makes use of the
precession of the
magnetization in the
demagnetizing field when
the magnetization acquires
an out-of-plane component
as it begins to process
around H'.
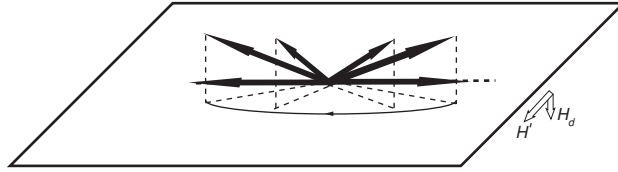
When $\alpha \ll 1$, the motion is lightly damped, and many precessions take place before alignment is achieved. When $\alpha \gg 1$, the motion is overdamped. Critical damping is when $\alpha = 1$. Then if a reverse field is applied, switching takes a time $t \approx 2/\gamma \mu_0 H$. Switching is rapid. For example, a moment with $\theta = 20°$ in a reverse field takes four precessions to reach $\theta = 170°$. If $\mu_0 H = 10$ mT, $t = 1$ ns when $g = 2$ ($\gamma = 1.76 \times 10^{11}$ s^{-1} T^{-1}). For switching the films it is possible to make use of the demagnetizing field, Fig. 9.7. Rapid switching of the magnetization of ferromagnetic thin film elements is important for spin electronics (§14.4).

9.2.3 Domain wall dynamics

Consider a $180°$ Bloch wall separating two domains with magnetization up or down along an anisotropy axis taken as the z axis. The magnetization turns in the yz-plane, making an angle θ with Oz, as shown in Fig. 7.6. From (7.15)

$$\frac{d^2\theta}{dx^2} = \frac{\pi^2}{\delta_w^2} \sin\theta \cos\theta, \tag{9.33}$$

where $\delta_w = \pi \sqrt{A/K_1}$ is the domain-wall width. The solutions are of the form $d\theta/dx = \pi \sin\theta/\delta_w$. Suppose now that a field $\boldsymbol{H}$ is applied along the positive z axis. This tends to drive the wall along Ox, exerting a pressure $2\mu_0 H M_s$ on it. If the field is applied for a time t, the wall acquires a velocity v_w, which we now calculate.

A consequence of $\boldsymbol{H}$ is to exert a torque on the spins in the wall. They precess around Oz with angular velocity $\omega_z = \mu_0 \gamma H$. After a short time, they all make a small angle ϕ with the z-plane. The magnetization of the wall acquires a component along) O_x, $M_x \approx M_s \phi \sin\theta$. The sheet of magnetization in turn creates a demagnetizing field $H_x = -M_x$, and it is this field that produces the torque needed to move the wall. The magnetization in the wall precesses around Ox with angular velocity $\omega_x = d\theta/dt = \mu_0 \gamma H_x = -\mu_0 \gamma M_s \phi \sin\theta$. The effect is to move the entire wall along Ox with velocity v_w. The angle ϕ accumulated in the time needed to damp the oscillation remains constant after $\boldsymbol{H}$ is switched off. In the moving wall, θ is a function of $x' = x - v_w t$. Hence

$$\frac{d\theta}{dx'} = -\frac{1}{v_w} \frac{d\theta}{dt} = \frac{1}{v_w} \mu_0 \gamma M_s \phi \sin\theta. \tag{9.34}$$

Domain-wall velocity in a thin film. The discontinuity at the Walker limit arises when the spins in the wall are driven faster than the Larmor precession frequency.
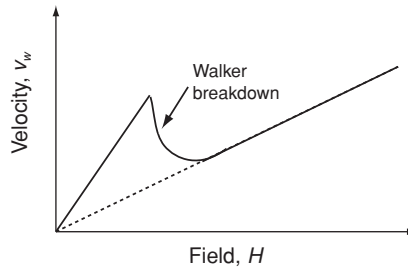
Since $\mathrm{d}\theta/\mathrm{d}x = \pi \sin\theta/\delta_w$ and $\phi = \mu_0 \gamma H t_0$, it follows that $v_w = 2\mu_0^2 \gamma^2 H M_s \delta_w / w_0 \alpha$. The ratio of impulse per unit area to velocity is an effective domain-wall mass per unit area:
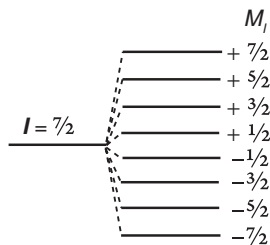
$$m_w = \frac{2\pi}{\mu_0 \gamma^2 \delta_w} \qquad (9.35)$$

This is known as the Döring mass. From data in Table 7.1, values of m_w for Fe and $Nd_2Fe_{14}B$ are 4×10^{-9} kg m^{-2} and 4×10^{-8} kg m^{-2}, respectively. Domain-wall dynamics is determined by this mass.

At low fields, the wall velocity v_w is proportional to the driving field beyond the depinning field H_p, with a constant of proportionality η_w known as the domain-wall mobility (7.31). In thin films, the mobility is limited by the Gilbert damping parameter α, so that $\eta_w = \mu_0 \gamma \delta_w / \alpha$ at high driving fields. The velocity of the wall collapses as the precession frequency of the spins approaches the ferromagnetic resonance frequency $\gamma B_0/2\pi$. The spins in the moving wall precess at a frequency v_w/δ_w; Walker breakdown occurs when this frequency hits the ferromagnetic resonance frequency, Fig. 9.8.

9.3 Nuclear magnetic resonance

The nucleus is the collection of protons and neutrons at the heart of every atom, which constitutes 99.98% of the mass of solids, liquids and gases. The magnetic properties of these and other elementary particles are listed in Table 9.2.

While the proton and the neutron possess the same spin angular momentum as the electron, $\hbar/2$, their magnetic moments are far smaller because of their much greater mass. The magnetic moments associated with the spin angular momentum can be written as $\mathrm{m}_n = g_n \mu_N I$, where the nuclear g-factors are $g_n = 5.586$ and $g_p = -3.826$ for the proton and neutron, respectively. The nuclear magneton μ_N is $e\hbar/2m_p$, 5.051×10^{-27} A m^2. The interacting protons and neutrons in the nucleus form an entity with angular momentum $I\hbar$, having $2I + 1$ degenerate states labelled with a magnetic quantum number M_I, analogous to the many-electron states of an atom. Whereas the excited states of the

Splitting of nuclear energy levels of ^{59}Co ($I = \frac{7}{2}$) in the hyperfine field.

		Charge	m/m_e	$\tau_{1/2}$	$I(\hbar)$	$\mathfrak{m}$	f_L(Hz T^{-1})
Proton	p	e	1836	Stable	$\frac{1}{2}$	2.793 μ_N	42.58×10^6
Neutron	n		1836	10.3 m	$\frac{1}{2}$	-1.913 μ_N	29.17×10^6
Electron	e	$-e$	1	Stable	$\frac{1}{2}$	-1.001 μ_B	27.99×10^9
Positron	e$^+$	e	1	Stable[a]	$\frac{1}{2}$	1.001 μ_B	27.99×10^9
Muon	μ^+	e	206.7	2.2 μs	$\frac{1}{2}$	0.00484 μ_B	135.5×10^6
Muon	μ^-	$-e$	206.7	2.2 μs	$\frac{1}{2}$	-0.00484 μ_B	135.5×10^6
Photon	ϕ			Stable	1		

Table 9.2. Magnetism of some elementary particles

[a] Positrons combine with electrons in condensed matter to produce two γ photons, each of energy 0.511 MeV.

many-electron atom lie 1–100 eV above the atomic ground state, the excited states of the many-nucleon nucleus lie 10 keV–10 MeV above the nuclear ground state. We rarely need to consider any but the nuclear ground state. Unlike electronic moments, which are usually negative (oppositely directed to the angular momentum on account of the negative electronic charge) the nuclear moments are usually positive.

On applying an external magnetic field, B_0 in the Oz-direction, the $2I + 1$ magnetic levels are Zeeman split which leads to the establishment of the Boltzmann populations. A small net magnetization is induced in the direction of the field, given by Curie's law. In a field of 1 T, the energy splitting for the proton $g_p \mu_N B$ is 2.8×10^{-26} J or 2 mK. The difference in population of the two levels is therefore less than 1 part in 10^5 at room temperature.

As for EPR, resonant transitions between the energy levels require an AC field to be applied in the xy-plane, perpendicular to the uniform field. The frequencies required for NMR are in the radio-frequency range (Table 9.3) rather than the microwave range, so the samples can be excited in a resonant coil with a few turns, rather than a waveguide.

The nucleus is surrounded by the electron shells of its atom, and by the other atoms in the sample, which have the effect of creating or modifying the electric and magnetic fields acting at the nucleus. NMR is very widely used in organic chemistry as a fingerprint spectroscopy for nonconducting organic compounds in the liquid state. The diamagnetic susceptibility of the inner electron shells tends to shield the nucleus slightly from the applied field, leading to a chemical shift of the resonance to slightly higher frequency ω_0. Chemical shifts are measured in parts per million, but the resonance linewidth may be a hundred times less, so a rich fund of molecule- and bond-specific chemical information is available. Modern high-resolution spectrometers use superconducting magnets which deliver B_0 in the range 12–20 T, and operate in the 500–800 MHz range.

In metals, the paramagnetic susceptibility of the conduction electrons shifts the resonance in the opposite direction. This is the Knight shift, discussed below. It is an effect of order 1%.

Table 9.3. Some nuclei of interest for magnetic resonance					
Nucleus	I^{parity}	(%)	$\mathfrak{m}\ (\mu_N)$	f_L(MHz T^{-1})	Q (10^{-28} m^2)
^{1}H	1/2+	99.9885	2.793	42.58	
^{2}H	1+	0.0115	0.857	6.54	0.0029
^{13}C	1/2+	1.07	0.702	10.71	
^{14}N	1+	99.632	0.404	3.08	0.0204
^{17}O	5/2−	0.038	−1.893	5.77	−0.0256
^{19}F	1/2+	100	2.627	40.05	
^{23}Na	3/2+	100	2.217	11.26	0.104
^{27}Al	5/2+	100	3.641	11.09	0.14
^{29}Si	1/2−	4.6832	−0.555	8.46	
^{31}P	1/2+	100	1.132	17.24	
^{33}S	3/2+	0.76	0.643	3.27	−0.0678
^{53}Cr	3/2−	9.501	−0.474	2.41	−0.150
^{55}Mn	5/2+	100	3.468	10.54	0.330
^{57}Fe	1/2+	2.19	0.091	1.38	
^{59}Co	7/2+	100	4.616	10.10	0.420
^{61}Ni	3/2−	1.14	−0.750	3.81	0.162
^{63}Cu	3/2+	69.17	2.226	11.29	−0.220
^{87}Rb	3/2w+	27.835	2.750	13.93	0.134
^{89}Y	1/2−	100	−0.137	2.09	
^{105}Pd	5/2−	22.33	−0.639	1.95	0.660
^{143}Nd	7/2−	12.81	−1.063	2.32	−0.630
^{147}Sm	7/2−	15.0	−0.813	1.76	−0.259
^{157}Gd	3/2−	15.65	−0.339	2.03	1.350
^{159}Tb	3/2+	100	2.008	9.66	1.432
^{163}Dy	5/2+	24.9	0.676	1.95	2.648

9.3.1 Hyperfine interactions

The atomic nucleus is a point probe of electric and magnetic fields at the very heart of the atom. Atoms in different crystallographic sites may be distinguished by their hyperfine interactions, which result from coupling of the electric and magnetic moments of the nucleus with these fields. Nuclei with $I \neq 0$ have a magnetic moment $g_n \mu_N I$, and the Zeeman splitting of the $(2I + 1)$ magnetic levels denoted by the nuclear magnetic quantum number $M_I = I$, $I - 1, \ldots, -I$ results from the action of the hyperfine field B_{hf} at the nucleus.

The complete Hamiltonian is

$$\mathcal{H}_{hf} = -g_n \mu_N \boldsymbol{I} \cdot \boldsymbol{B}_{hf} - eQV_{zz}\{[3I_z^2 - I(I + 1)] + \eta(I_x^2 - I_y^2)\}/[4I(2I - 1)], \tag{9.36}$$

where the first term is the magnetic hyperfine interaction and the second term represents the interaction of the electric quadrupole moment of the nucleus with the electric field gradient V_{zz}. Higher-order moments of the nuclear charge are

Temperature dependence of the hyperfine field of an antiferromagnet. The data are for α-Fe_2O_3 which exhibits a spin reorientation transition at T_M. (F. van der Woude et al., *Phys. Stat. Sol.* **17**, 417 (1966).)
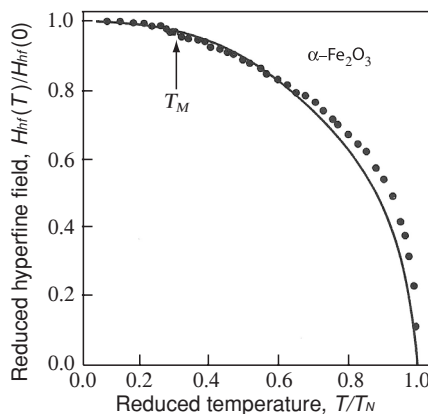
negligible. There are several contributions to the hyperfine field B_{hf}; one is the Fermi contact interaction of the nucleus with the unpaired electron density at its site. Unpaired electrons are largely in $3d$ and $4f$ shells which have no electron density at the nucleus, but they polarize the $1s$, $2s$ and $3s$ core shells which do have some charge density there. The core polarization contribution is largest for $3d$ elements; it is about -11 T μ_B^{-1} in iron and cobalt, and 4 T μ_B^{-1} in the rare-earths. A further contribution comes from the spin-polarized $4s$ or $6s$ conduction electrons. For non-S state ions there are also orbital and dipolar contributions, $B_{orb} = -2\mu_0\mu_B\langle r^{-3}\rangle\langle \boldsymbol{L}\rangle/h$ and $B_{dip} = -2\mu_0\mu_B\langle r^{-3}\rangle\langle \boldsymbol{S}\rangle\langle 3\cos^2\theta - 1\rangle/h$, produced by the unquenched orbital angular momentum and the non-spherical atomic spin distribution, respectively. In non-S-state rare-earths, these contributions reach values of several hundred teslas. At lattice sites which do not have cubic symmetry, there may also be a dipolar contribution from the moments of the atoms on the rest of the lattice, which is of order 1 T.

Normally, *no* magnetic hyperfine splitting is observed in the paramagnetic state. The reason is that the fluctuations of the atomic moment in a paramagnet are much faster than the nuclear Larmor precession frequency in the hyperfine field $f_L \approx 10^9$ Hz. Dilute paramagnetic salts of non-S-state rare-earth ions may be an exception. There the Larmor precession frequency is several gigahertz on account of the orbital and dipolar contributions, and if the crystal field stabilizes a $\pm M_J$ ground state with $M_J > 3$ the fluctuation time can be slow at low temperature because the $M_J \rightarrow -M_J$ transitions are suppressed on account of the large change of orbital angular momentum $\Delta M_J = 2J$ involved.

The magnetic hyperfine field in magnetically ordered material faithfully follows the ordered moment, and it falls to zero at the Curie or Néel temperature. Accurate values of the critical exponent β are obtained in this way, which is especially valuable for antiferromagnets, Fig. 9.9.
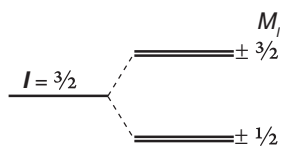
The second term in (9.36) represents the electrostatic coupling of the nuclear quadrupole moment Q with the electric field gradient at the nucleus $V_{ij} = \mathrm{d}^2 V/\mathrm{d}x_i\,\mathrm{d}x_j$. Any nucleus with $I \geq \frac{3}{2}$ has a quadrupole moment, and the electric quadrupole interaction, represented by the second term in (9.36), has the effect

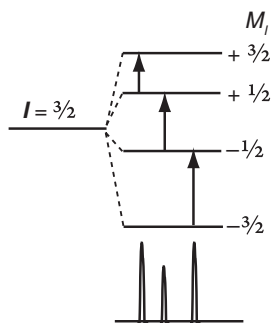| Table 9.4. Some values of the Knight shift	
	$\mathcal{K}$ (%)
^{22}Na	0.11
^{23}Al	0.16
^{53}Cr	0.69
^{63}Cu	0.24
^{105}Pd	−3.00

of separating the pairs of levels with different $|M_I|$. The electric field gradient at the nucleus can be diagonalized by a suitable choice of axes; only two of the three components (V_{xx}, V_{yy}, V_{zz}) are independent. Conventionally, the biggest is labelled V_{zz} and the asymmetry parameter is defined as $\eta = (V_{xx} - V_{yy})/V_{zz}$. These quantities in S-state ions are related to the second-order crystal field acting on the electronic shell: $V_{zz} \approx A_2^0$, $\eta \approx A_2^2$. The inner electron shells greatly amplify the electric field gradient produced by the lattice $(V_{zz})_{latt}$, and they shield the atomic charge $(V_{zz})_{val}$ contribution.

$$V_{zz} = (1 - \gamma_\infty)(V_{zz})_{latt} + (1 - R)(V_{zz})_{val}, \tag{9.37}$$

Quadrupole splitting of the energy levels of a nucleus with $I = \frac{3}{2}$.

modifying the field gradient at the nucleus. The factors γ_∞ and R are the Sternheimer antishielding and shielding factors, respectively. For example, values for ^{57}Fe are $\gamma_\infty = -9.14$ and $R = 0.32$.

The absorption of radio-frequency radiation by nuclei such as ^{14}N which are subject to an electric field gradient is nuclear quadrupole resonance. As for zero field splitting in epr, no applied magnetic field is required. The order of magnitude of the magnetic and electric hyperfine interactions is 10^{-6} eV (10 mK). Some nuclei of interest for nuclear quadrupole resonance are included in Table 9.3.

The Knight shift of a paramagnetic metal is related to the magnetically induced hyperfine field, which may be expressed in terms of the hyperfine coupling constant A and the susceptibility. The energy of the nucleus in an applied field B_0 is

$$\varepsilon = (-\gamma_n \hbar B_0 + A\langle s_z \rangle)M_I. \tag{9.38}$$

A nucleus with $I = \frac{3}{2}$ subject to magnetic and electric hyperfine interactions, and the corresponding hyperfine spectrum.

The first term is the Zeeman interaction of the nucleus with the applied field, and the second is the interaction with the electrons in the spin-polarized conduction band. The nuclear gyromagnetic ratio is $\gamma_n = g_n e/2m_p$. Now $M = ng\mu_B \langle s_z \rangle = \chi_P B_0/\mu_0$, where n_c is the conduction electron density, g is the electronic g-factor and χ_P is the Pauli susceptibility. Hence $\varepsilon = -\gamma_n \hbar B_0(1 + \mathcal{K})M_I$, where

$$\mathcal{K} = -A\chi_P/n_c g\mu_B \gamma_n \hbar \tag{9.39}$$

is the Knight shift. Some values of $\mathcal{K}$ are given in Table 9.4.

9.3.2 Relaxation

Consider the magnetization M^n of a system of nuclei: $M^n = n\langle m_n \rangle$, where n is the number of nuclei per unit volume. When the system is perturbed, it tends to return to its equilibrium state where M_0^n is along Oz with a characteristic relaxation time in a similar way to the magnetization of a system of electrons discussed in §9.1. However, the nuclei are weakly coupled to the lattice, so the longitudinal, spin-lattice relaxation time T_1 is much longer than it was for electrons: $M_z^n(t) = M_z^n(0) + [M_0^n - M_z^n(0)][1 - \exp(-t/T_1)]$. Thus

$$\frac{dM_z^n(t)}{dt} = \frac{M_0^n - M_z^n(t)}{T_1}. \tag{9.40}$$

The torque acting on a nuclear moment m_n is $m_n \times B$, which is equal to the rate of change of angular momentum $d(\hbar I)/dt$. Hence $dm_n/dt = \gamma_n m_n \times B$. The nuclear magnetization for an ensemble of nuclei M^n is $\langle m_n \rangle$. The z component of the equation of motion in the absence of irradiation is

$$\frac{dM_z^n}{dt} = \gamma_n (M^n \times B)_z + \frac{M_0^n - M_z^n}{T_1}. \tag{9.41}$$

In other words, the nuclear magnetization precesses around Oz, while relaxing towards the equilibrium value M_0^n. The values of T_1 for protons range from milliseconds, up to about 1 s in pure water.

Spin-lattice relaxation in metals mostly involves the conduction electrons. The inverse relaxation time $1/T_1$ is proportional to temperature, and to the Knight shift, a result known as the Korringa relation:

$$\frac{1}{T_1} = \mathcal{K}\left(\frac{\gamma_n}{\gamma}\right)^2 \frac{4\pi k_B T}{\hbar}. \tag{9.42}$$

The equations of motion for the x and y components are different from (9.41). There is no nonzero equilibrium value for these components, and they decay with a relaxation time known as the transverse or spin–spin relaxation time T_2. Hence

$$\frac{dM_x^n}{dt} = \gamma_n (M^n \times B)_x - \frac{M_x^n}{T_2},$$
$$\frac{dM_y^n}{dt} = \gamma_n (M^n \times B)_y - \frac{M_y^n}{T_2}. \tag{9.43}$$

T_2 is a measure of the time for which the moments contributing to M_x^n and M_y^n precess in phase with each other. It is the spin dephasing time, due to the fact that nuclear moments in different parts of the sample all experience slightly different magnetic fields, and therefore precess at different rates. If we consider that the local field fluctuations are due to the dipole fields of nearby nuclei, $H_{dip} \approx m_n/4\pi r^3$. Taking $r \approx 0.2$ nm and $m_n = \mu_N$ gives $\mu_0 H_{dip} \approx 60$ μT. The dephasing time T_2 is the time taken to precess through a radian in the

Illustration of the basic relaxation processes in NMR. The longitudinal relaxation time T_1 for alignment of the moments with the field direction is longer than the dephasing time T_2 of the in-plane magnetization due to slightly different precession frequencies of the different moments.
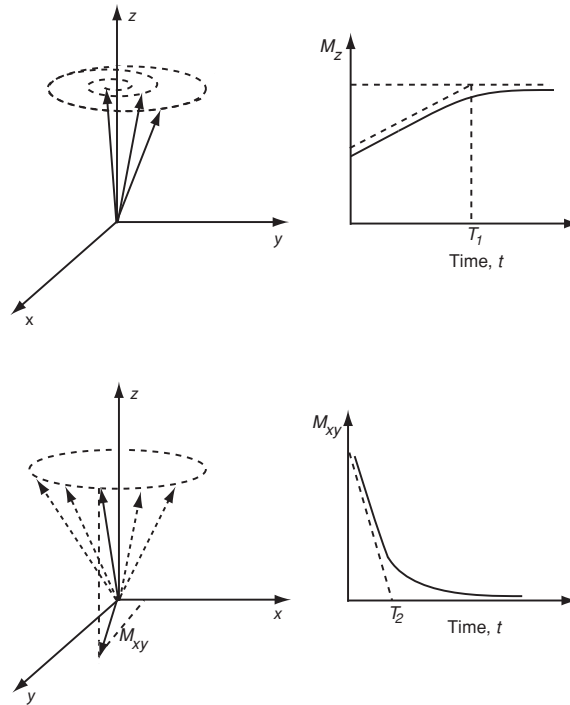
random field, at an angular frequency $\omega = \gamma_n \mu_0 H_{dip}$. Hence $T_2 \approx \hbar / \mu_0 \mu_N H_{dip} \approx 30$ μs.

Inhomogeneity of the applied field B_0 may also contribute to T_2. The combined time constant T_2^* is given by

$$\frac{1}{T_2^*} = \frac{1}{T_2} + \frac{1}{T_2^{inho}}. \tag{9.44}$$

Unlike the relaxation of the longitudinal component M_z^n, there is no exchange of energy with the surroundings associated with the transverse components M_x^n and M_y^n. Equations (9.41) and (9.43) are known as the Bloch equations. They are phenomenological relations, first proposed by Felix Bloch in 1946. The longitudinal and transverse relaxation effects are illustrated in Fig. 9.10.

Adding in the AC field, of which we consider only the clockwise-rotating component $\boldsymbol{b}_1(t) = b_1(\mathbf{e}_x \cos \omega t + \mathbf{e}_y \sin \omega t)$ which can excite the resonance, Bloch's equations become

$$\frac{dM_x^n}{dt} = \gamma_n \left(M_y^n B_0 - M_z^n b_1 \sin \omega t \right) - \frac{M_x^n}{T_2}, \tag{9.45}$$

$$\frac{dM_y^n}{dt} = \gamma_n \left(M_z^n b_1 \cos \omega t - M_x^n B_0 \right) - \frac{M_y^n}{T_2},$$

$$\frac{dM_z^n}{dt} = \gamma_n b_1 \left(M_x^n \sin \omega t - M_y^n \cos \omega t \right) + \frac{M_0^n - M_z^n}{T_1}.$$

Rotating frame   It is helpful to think of resonance experiments in a set of axes x', y', z' that rotate at an angular velocity $\boldsymbol{\Omega}$ relative to the laboratory frame x, y, z. The time derivatives of the unit vectors $\mathbf{e}_i$, $i = x, y, z$ in the rotating frame are $\mathrm{d}'\mathbf{e}_i/\mathrm{d}t = \boldsymbol{\Omega} \times \mathbf{e}_i$. The time derivative of a general vector A in the rotating frame is related to its derivative in the stationary frame by

$$\frac{\mathrm{d}'A}{\mathrm{d}t} = \frac{\mathrm{d}A}{\mathrm{d}t} + \boldsymbol{\Omega} \times A.$$

We are interested in the magnetization M, subject to a uniform field B_0 along Oz. The z axis is common to the laboratory and rotating frames. Thus

$$\frac{\mathrm{d}'M}{\mathrm{d}t} = \gamma_n M \times B_0 + \boldsymbol{\Omega} \times M = \gamma_n M \times \left(B_0 - \frac{\boldsymbol{\Omega}}{\gamma_n} \right).$$

It is as if the magnetization in the rotating field were subject to an effective magnetic field $B_0' = (B_0 - \boldsymbol{\Omega}/\gamma_n)$. When $\Omega = \gamma_n B_0$ is the Larmor precession frequency ω_0, there is no effective field and the magnetization appears to be stationary in the rotating frame.

The in-plane rotating field $b_1(t)$ becomes a static field b_1 directed along Ox in a frame rotating with angular velocity ω. Rewriting the Bloch equations in the rotating frame with $z' = z$, we find

$$\frac{\mathrm{d}M_{x'}^n}{\mathrm{d}t} = \gamma_n M_y^n B_0' - \frac{M_{x'}^n}{T_2},$$

$$\frac{\mathrm{d}M_{y'}^n}{\mathrm{d}t} = \gamma_n \left(M_{z'}^n b_1 - M_{x'}^n B_0' \right) - \frac{M_{y'}^n}{T_2}, \qquad (9.46)$$

$$\frac{\mathrm{d}M_{z'}^n}{\mathrm{d}t} = -\gamma_n M_{y'}^n b_1 + \frac{M_0^n - M_{z'}^n}{T_1},$$

where $B_0' = (\omega_0 - \omega)/\gamma_n$. These equations can be solved to give expressions for $M_{x'}$, $M_{y'}$, $M_{z'}$ in the steady state, when the time derivatives are zero. Furthermore, provided we stay in the limit of low excitation field b_1, far from saturation ($\gamma b_1 \ll T_1, T_2$), the resonance is independent of T_1:

$$M_{x'}^n = \frac{\gamma_n b_1'(\omega_0 - \omega)T_2^2}{1 + (\omega_0 - \omega)^2 T_2^2} M^n,$$

$$M_{y'}^n = \frac{\gamma_n b_1 T_2}{1 + (\omega_0 - \omega)^2 T_2^2} M^n, \qquad (9.47)$$

$$M_{z'}^n = M^n,$$

where $M^n = \chi^n B_0/\mu_0$. The in-phase component of the magnetization $M_{x'}$ and the out-of-phase component $M_{y'}$ are plotted in Fig. 9.11.

Written in terms of susceptibility, the magnetization of the system subject to an in-plane oscillating field of amplitude $2b_1$ in the laboratory frame is

$$M_x = 2b_1(\chi' \cos \omega t + \chi'' \sin \omega t).$$

The Lorentzian lineshape of the resonance at the Larmor precession frequency ω_0. The in-phase component $M_{x'}$ is dispersive, while the out-of-phase component $M_{y'}$ is absorptive.
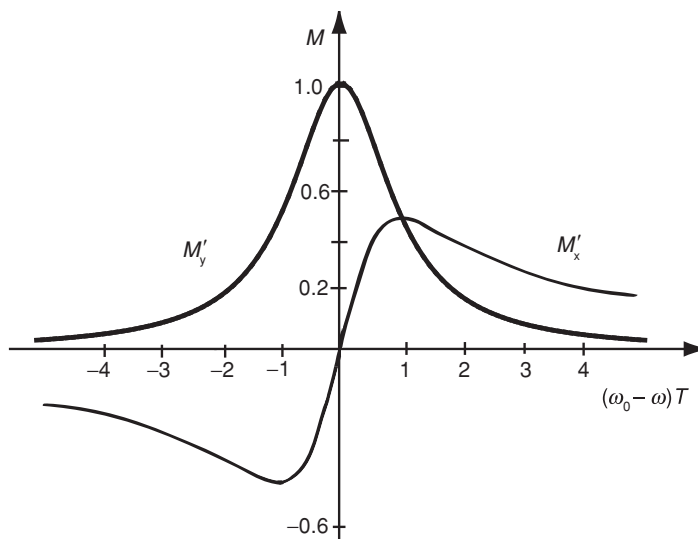
The components of the magnetization in the rotating frame $M_{x'}$ and $M_{y'}$ are then proportional to χ' and χ'', the components of the complex susceptibility $\chi = \chi' - i\chi''$. The power absorbed per unit volume of the system is $\mathcal{P} = \omega\chi'' b_1^2/\mu_0$.

The longitudinal relaxation time in the rotating frame is $T_{1\rho}$. It reflects molecular motion in macromolecules.

Equations (9.41) and (9.43) are also applicable to EPR and FMR where they are known as the Bloch–Bloembergen equations. T_1 and T_2 are then the spin-lattice and spin–spin relaxation times for the electronic system The resonance linewidth is given by $\Delta B = 2/(\gamma T_2)$: it is also related to the Gilbert damping parameter α by $\Delta B = 2\alpha\omega_0/\gamma$.

9.3.3 Pulsed NMR

Most modern NMR spectrometers apply the radio-frequency field in precisely timed bursts, rather than continuously. $b_1(t)$ is stationary in the rotating-axis frame at resonance, so it is possible to precess the magnetization of the sample M^n around Ox' through any desired angle in the $y'z'$-plane by choosing the length of the pulse. A π pulse, for example, reverses the magnetization, whereas a $\pi/2$ pulse causes precession through a quarter turn, and brings the magnetization into the xy-plane. The pulse lengths are generally shorter than the relaxation times T_1 and T_2.

A single $\pi/2$ pulse is especially useful, as it flips the magnetization from the z axis to the xy-plane, where it continues to precess at the Larmor frequency; Larmor precession does not depend on the angle between the magnetization and the field B_0. As the magnetization precesses, it induces a radio-frequency signal

Figure 9.12

(a) A free induction decay for a sample with protons present in several different environments. (b) The Fourier transform shows the spectrum of component frequencies in the free induction decay. The horizontal axis shows the chemical shift of the resonance frequency in parts per million. (Data courtesy of V. J. McBrierty.)
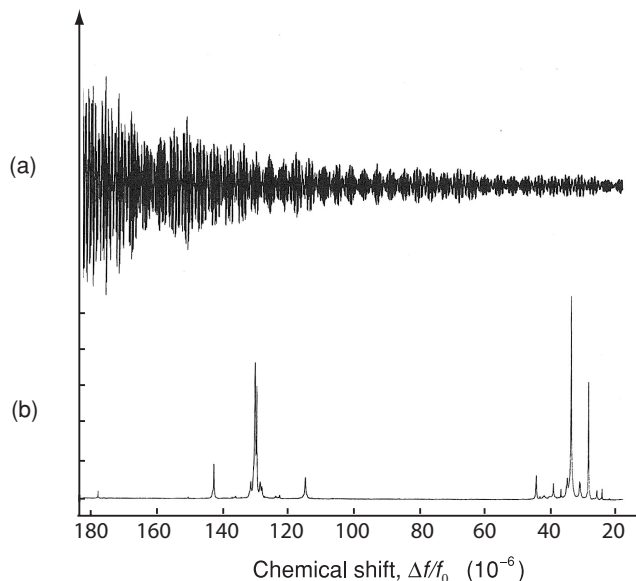
in the coil that was used to create the pulse, which is damped by the progressive dephasing of the contributions of individual nuclei which see slightly different magnetic fields. This signal is known as the free induction decay, Fig. 9.12. It allows T_2 to be measured directly. A fast Fourier transform of the free induction decay gives the frequency spectrum, and the chemical shifts of the constituent nuclei can be identified.

Spin echo The benefits of high resolution might seem to depend on our ability to build a magnet capable of producing a perfectly uniform magnetic field B_0 over the whole volume of the sample. Luckily, that is not true, thanks to an ingeneous pulse sequence invented by Erwin Hahn in 1950. The spin-echo method uses two pulses. First a $\pi/2$ pulse switches the magnetization into the plane along Oy and a free induction decay is measured which reflects both the inherent field fluctuations in the sample, as well as any inhomogeneities in field produced by the magnet. Then after a time τ a π pulse is applied, which flips the spins around Ox and reverses their order as they continue to precess, as shown in Fig. 9.13. The spins which were precessing faster now find themselves lagging behind their slower counterparts, but they catch up the delay, and all spins find themselves coming together along the y-direction after a time 2τ, producing the 'spin echo'.

T_1 can be measured by first applying a π pulse to flip the magnetization, and then using a $\pi/2$ pulse after a variable time delay τ to determine the magnitude of the magnetization measured in the free induction decay $M(\tau)$. A curious feature of the nonequilibrium population distributions that can be achieved with spin systems is spin temperature. This is the fictitious temperature T^* at which the population distribution measured at some instant would be in
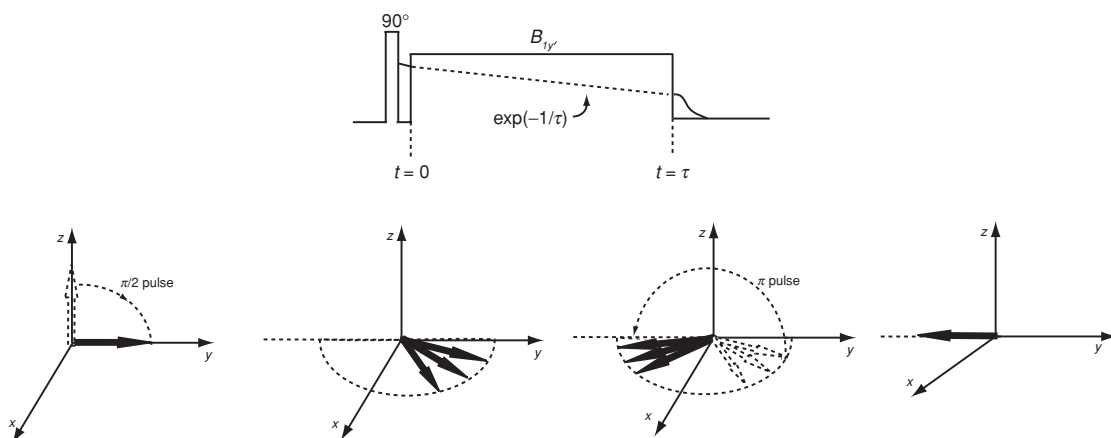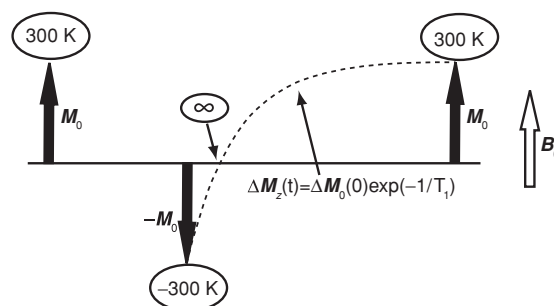
Figure 9.13

The spin-echo measurement.

Figure 9.14

Recovery of the magnetization in the direction of the uniform field B_0 following a π pulse at room temperature. Some spin temperatures are circled.

equilibrium. The population of the M_I sublevels is described by a Boltzmann distribution with the temperature equal to T^* rather than T. The spins can equilibrate with each other at a temperature quite different from the lattice temperature when $T_2 \ll T_1$. After inverting the magnetiztion with a π pulse at 300 K, for example, the spin temperature flips to -300 K. It then becomes increasingly negative, diverging to $-\infty$ as the moment crosses the xy-plane, and it eventually reaches 300 K again when $t \gg T_1$, as shown on Fig. 9.14.

Spin locking of the moments in the rotating frame is achieved with a $\pi/2$ pulse along Ox', followed by a $\pi/2$ phase shift of the radio-frequency field, so that it lies along Oy'. This aligns M_0 and b_1 in the rotating frame, allowing measurement of $T_{1\rho}$. The tendency for the magnetization to dephase is suppressed, and the large population imbalance in relation to the field produces a low effective spin temperature $T^* = T(b_1/b_0)$. For example, if $B_0 = 1$ T and $b_1 = 1$ mT, the spin temperature is 300 mK.

Many other pulse sequences devised by practitioners of NMR are described in specialist texts.

Finally, we return to the concept of motional narrowing. When some component of the hyperfine field acting on a nucleus is fluctuating because of temperature or diffusive motion, motional averaging affects the spectrum provided the fluctuation frequency is comparable to or greater than the spectral width arising from the interactions. For magnetic hyperfine interactions, the fluctuation frequency is the Larmor precession frequency. We have seen how paramagnetic fluctuations of the magnetization are averaged out when their frequency exceeds the Larmor frequency in the hyperfine field. Similarly, line broadening associated with dipole fields created by neighbouring nuclei in liquids, for example, averages out when the diffusion frequency exceeds the frequency associated with the dipole field. This permits the observation of very narrow resonance lines in liquids, with relative linewidths of 10^{-8}. A similar effect is achieved in solids by the technique of magic angle spinning, where anisotropic interactions such as dipole coupling and quadrupole coupling which vary as $(3\cos^2\theta - 1)$ are averaged out by spinning the sample around an axis inclined at an angle of $\cos^{-1}(1/\sqrt{3}) = 54.7°$ with Oz.

9.4 Other methods

9.4.1 Mössbauer effect

Mössbauer spectroscopy is based on the 1958 discovery by Rudolf Mössbauer that it is possible for a nucleus of ^{191}Ir to decay without recoil from its first excited state to its ground state by γ-ray emission, whenever the nucleus belongs to an atom bound in a solid. Momentum has to be conserved *on average*, but lattice momentum must be taken up by the creation of phonons. In quantum mechanics, zero-phonon, one-phonon, two-phonon, . . . , events all have finite probabilities. The recoilless fraction f_M is the fraction of decays where γ-rays are emitted without recoil in a zero-phonon process:

$$f_M = e^{(-\varepsilon_\gamma \langle x^2 \rangle / \hbar^2)}, \tag{9.48}$$

where $\langle x^2 \rangle$ is the mean-square thermal displacement of the nucleus and ε_γ is the energy of the γ-ray. A similar *Debye–Waller factor* governs the intensity of elastic X-ray and neutron scattering in solids. The Mössbauer effect is simply due to these zero-phonon events having a finite probability.

Mössbauer spectroscopy is based on the γ-rays emitted or absorbed in zero-phonon processes in transitions between the nuclear excited state and the ground state. Like optical spectroscopy, it requires a source, an absorber and a means of modulating the emitted photon energy. The source is a solid containing a radioactive isotope which decays with a half-life $\tau_{1/2}$ to populate a low-lying nuclear excited state, which in turn decays rapidly by emitting an unsplit gamma line. The conditions are stringent. The excited state must be at no more

Table 9.5. Some suitable isotopes for Mössbauer spectroscopy

Isotope	Abundance (%)	source	$\tau_{\frac{1}{2}}$	$t_{\frac{1}{2}\gamma}$ (keV)	$t_{\frac{1}{2}}$ (ns)	g_n	I^{parity}	Q	g_e	I_e^{parity}	Q_e
^{57}Fe	2.12	^{57}Co (ec)	270d	14.4	98.0	0.0906	$1/2^-$	–	−0.155	$3/2^-$	0.16
^{61}Ni	1.2	^{61}Co (β^-)	99m	67.4	5.3	−0.750	$3/2^-$	0.162	0.47	$5/2^-$	−0.30
^{119}Sn	8.6	^{119m}Sn (IT)	293d	23.9	18.0	3.359	$1/2^+$	–	2.35	$3/2^+$	−0.13
^{149}Sm	13.8	^{149}Eu (ec)	90d	22.5	7.3	−0.672	$7/2^-$	0.075	−0.620	$5/2^-$	0.40
^{151}Eu	47.8	^{151}Sm (β^-)	90y	21.6	9.6	3.465	$5/2^+$	0.903	2.587	$7/2^+$	1.51
^{155}Gd	14.8	^{155}Eu (β^-)	4.8y	86.5	6.5	−0.259	$3/2^-$	1.270	−0.515	$5/2^+$	0.16
^{161}Dy	18.9	^{161}Tb (β^-)	6.9d	25.7	29.1	−0.481	$5/2^-$	2.507	0.59	$5/2^+$	1.36

Figure 9.15

Nuclear decay scheme of ^{57}Co which undergoes (n,γ) decay, populating the 14.1 keV excited state of ^{57}Fe. These γ-rays are resonantly absorbed in an absorber containing ^{57}Fe. Hyperfine structure in the absorption spectrum is revealed by modulating the energy of the source by moving it with constant acceleration with an electromagnetic transducer. A six-level hyperfine spectrum of a ferromagnetic αFe absorber is illustrated.
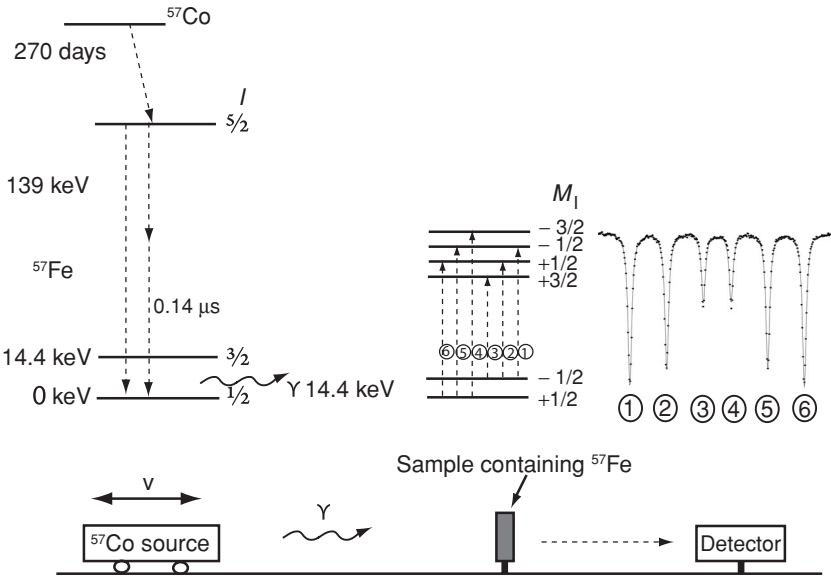

than about 30 keV, or else the recoilless fraction at room temperature becomes vanishingly small. Nature must provide a convenient radioactive precursor, if we are to avoid recourse to a synchrotron source. Some useful nuclei, and their radioactive precursors are listed in Table 9.5. Luckily for magnetism, the best example is an iron isotope, ^{57}Fe. Details are featured in Fig. 9.15. The source is ^{57}Co, which has a half-life $\tau_{1/2}$ of 270 days, and the energy ε_γ of the transition from the excited state to the ground state is 14.4 keV. Mössbauer spectroscopy is usually measured in transmission; a single-line source is energy-modulated by moving it with velocity v ($\approx$ cm s^{-1}) so that it undergoes a Doppler shift $\Delta\varepsilon = \varepsilon_\gamma v/c$. The absorption of γ-rays is measured as a function of velocity. The absorption linewidth determined by the lifetime $t_{1/2}$ of the nuclear excited state is 0.19 mm s^{-1} for the 98 ns $I = 3/2$ excited state of ^{57}Fe.

Both magnetic hyperfine splitting and electric quadrupole interactions are observed, for ^{57}Fe on account of the quadrupole moment of the excited state. The corresponding energy splittings are shown in Fig. 9.15. In addition, there is another interaction, unmeasurable in NMR, known as the isomer shift. It arises because the nucleus is a slightly different size in its excited state, and there is a shift of the resonance line due to the Coulomb interaction, depending on the difference in electron density at the nucleus in the source and absorber. Different absorbers have different isomer shifts δ_{IS} relative to a source, and it is possible to infer the charge state of the absorber ion, for example, Fe^{2+} or Fe^{3+}. Further details are provided in §10.2.3.

9.4.2 Muon spin rotation

Muons are unstable spin-$\frac{1}{2}$ particles with charge $\pm e$ which have a mass $m_\mu = 206.7\ m_e$. Their half-life is $\tau_\mu = 2.2\ \mu s$. The positive muon is quite useful as a probe of magnetic solids because it occupies an interstitial site where it experiences the local magnetic field. Negative muons are like heavy electrons and they bind closely to atomic nuclei, which is useful for cold fusion. Muon beams are produced in accelerators, where high-energy protons collide with a target producing pions, which decay into muons 26 ns later:

$$\pi^+ \longrightarrow \mu^+ + \nu_\mu.$$
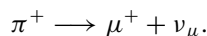
Remarkably, the muons produced are fully spin polarized; this is because the pion has no spin and the muon neutrino ν_μ has its spin antiparallel to its momentum and so the muon also has its spin antiparallel to its momentum.

The muons are created with energy in the MeV range, but they are rapidly thermalized on entering a solid specimen without loss of spin polarization. The final resting place of the muon in the sample is an interstitial site far from the track of radiation damage produced in the early stages of thermalization. After a time t there is a probability proportional to $1 - e^{-t/\tau_\mu}$ that the muon will have decayed into a positron and two neutrinos:

$$\mu^+ \longrightarrow e^+ + \nu_e + \bar{\nu}_\mu.$$
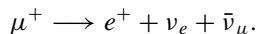
The positron emerges in a direction related to the spin direction of the parent muon. If a magnetic field is applied in the perpendicular direction, the muon precesses around this field at its Larmor frequency of 135 MHz T^{-1} before decaying to emit the positron.

There might only be a single muon in the sample at a given instant, but by averaging over many events, curves showing the intensity oscillations of the positron flux in fixed detectors can be recorded and the precession frequency of the muon is determined. The muon precesses equally well around the internal magnetic field present at its interstitial site and the main use of muon spin rotation (μSR) in solids is to study these local fields, which are in the range

10^{-4}–1 T. The spin depolarization of the muon can be used to probe spin dynamics both above and below the Curie temperature of a ferromagnet.

FURTHER READING

A. Guimares, *Magnetism and Magnetic Resonance in Solids*, New York: Wiley-Interscience (1998). An introduction to magnetic resonance in solids.

C. P. Schlichter, *Principles of Magnetic Resonance* (third edition), Berlin: Springer (1990).

A. Abragam, *Principles of Nuclear Magnetism*, Oxford: Oxford University Press (1961). The definitive text.

A. Abragam and B. Bleany, *Electron Paramagnetic Resonance of Transition Ions*, Oxford: Oxford University Press (1970).

N. N. Greenwood and T. C. Gibb, *Mössbauer Spectroscopy*, London: Chapman and Hall (1971). An account of the principles, followed by data on many materials for all the main resonances.

EXERCISES

9.1   Sketch the EPR spectrum of an Fe^{3+} ion ($S = \frac{5}{2}$) in a site with crystal field parameter $D = -0.05$ K. Assume a microwave frequency of 9.0 GHz.

9.2   Why does the entire, instantaneous hyperfine field split the electronic energy levels in an EPR experiment, while only its thermal average is effective for splitting the nuclear energy levels in an NMR experiment?

9.3   Estimate the Walker breakdown field for a single-crystal film of $Nd_2Fe_{14}B$, which has its c axis perpendicular to the plane of the film. Assume a damping factor $\alpha = 0.1$.

9.4   Sketch the Mössbauer spectrum for ^{155}Gd at 4K. The hyperfine field is 35 T.

9.5   Discuss the possibility of measuring the gravitational acceleration of photons using the Mössbauer effect.